ELSEVIER

Journal of Alloys and Compounds 401 (2005) 34–40

Journal of ALLOYS AND COMPOUNDS

www.elsevier.com/locate/jallcom

Inequality of quenched and high temperature structure of lithium deficient $LiMn_2O_4$

P. Piszora *

Laboratory of Magnetochemistry, Adam Mickiewicz University, Grunwaldzka 6, PL-60780 Poznań, Poland

Received 15 October 2004; received in revised form 15 February 2005; accepted 16 February 2005
Available online 3 June 2005

Abstract

Structural characterization of the new low temperature polymorph of the lithium-deficient lithium–manganese spinel, synthesized and quenched from 1073 K has been obtained by Rietveld structure refinements of X-ray powder diffraction data recorded using synchrotron radiation. A slight lithium ions deficiency causes formation of the tetragonal phase provided that the samples obtained at high temperature are rapidly quenched in the solid CO_2. The new phase has a tetragonally distorted spinel structure at 140 K with a space group $F4_1/ddm$, unit cells of $a = 8.33180(6)$ Å and $c = 8.08617(7)$ Å. On heating, at 280 K, the tetragonal phase transforms to cubic spinel structure (*Fd3m*) and it remains cubic up to 1163 K.

Keywords: Electrode materials; Crystal structure and symmetry; X-ray diffraction; Synchrotron radiation; Lithium-ion batteries; Tetragonal $LiMn_2O_4$

1. Introduction

The demands for the lighter, smaller and more powerful secondary battery increase with the population of electronic devices such as cellular phone, notebook computer and video camera. Nowadays the lithium secondary battery is one of the most promising for the portable electronic devices. $LiMn_2O_4$ spinel oxide is a good candidate material for a cathode of lithium secondary battery due to its economical and non-toxicity advantages.

At room temperature the crystal structure of $LiMn_2O_4$ belongs to the *Fd3m* space group of a cubic system. The distribution of cations in $LiMn_2O_4$ is represented by the following ionic formula: $Li^{+}{}_{8a}[Mn^{3+}Mn^{4+}]_{16d}O^{2-}{}_4$, where *8a* and *16d* refer to the tetrahedral and octahedral sites of the cubic spinel structure.

Many fast synthesis methods, such as microwave technique [1], pulsed laser deposition [2,3] and ultrasonic spray pyrolysis [4,5], are applied recently in order to obtain $LiMn_2O_4$ with the good electrochemical Li charge–discharge cycle performance. The rapid thermal treatment is very often applied in the thin film electrode fabrication for rechargeable microbatteries [6–8]. Nevertheless, the short time thermal annealing is followed often by the fast cooling of the samples and leads to the preservation of the average Mn valence and the high temperature Mn cations distribution.

The research of the lithium–manganese spinel at high temperature has been hitherto undertaken, but with contradictory results (Table 1). Several authors have observed the formation of tetragonal spinel phases at $1053 < T < 1188$ K [9–16], whereas no evidence for their existence up to 1253 K has been found by other authors [17–20]. The tetragonally distorted lithium-manganese spinel oxide has been observed, but only for samples partially decomposed to the lithium-deficient $Li_{1-x}Mn_{2+x}O_4$, and to the lithium-rich phase, e.g. Li_2MnO_3.

The thermal stability of $LiMn_2O_4$ had been studied in-situ by Thackeray et al. [9] using X-ray diffractometer equipped with a high temperature attachment. They have found that in the temperature region of 1113–1273 K the lithium-rich Li_2MnO_3 phase coexists with the tetragonal lithium deficient lithium–manganese spinel ($c/a = 1.02$ at 1073 K). At the temperature above 1233 K $LiMnO_2$ is created, whereas

* Tel.: +48 61 8291262; fax: +48 61 8658008.
E-mail address: pawel@amu.edu.pl.

0925-8388/$ – see front matter © 2005 Elsevier B.V. All rights reserved.
doi:10.1016/j.jallcom.2005.02.059

Table 1
The unit-cell parameters, *c*/*a* ratio and experimental condition for lithium–manganese spinel quenched or investigated at high temperature

References	Preparation conditions				Sample labels and details	Diffraction setup	*a* [Å][a]	*c* [Å][a]	*c*/*a*
	Substrates and preparation temperature	Atmosphere	Final temperature [K]	Sample treatment					
[18]	$Li_2CO_3 + Mn_2O_3$,	O_2	1173	Fast cooled 100 K/min	A $\delta = 0.132$	Neutron (TOF) KENS, KEK	8.24609(17)		
	$Li(CH_3COO)\cdot LiOH\cdot H_2O \rightarrow MnO_x$ 743 K × 3	Air	1023	60 K/min	B $\delta = 0.088$		8.24203(14)		
		Air/O_2	1023	60 K/min	C $\delta = 0.00$		8.23634(13)		
[9]	γ-MnO_2 + $LiOH\cdot H_2O$, 1153 K		873–1473	In situ	+Li_2MnO_3 for 1113 K ≤ *T* ≤ 1273 K + $LiMnO_2$ for 1233 K ≤ *T* ≤ 1393 K	Simens D5000 Cu Kα, Buhler HDK S1 high temperature attachment	Not published	Not published	1.02
[19]	$Li_2CO_3 + MnCO_3$, 823 K/1 day, 1023 K/3 days	O_2	1023	Quenched	$0.00 < \delta < 0.04$, cubic	Rint 2500 V (Rigaku) CuKα	[c]		
[20]	LiOH + Mn_3O_4, 803 K/5 h, 973 K/24 h, 1073 K/24 h	Air	1073	Quenched	A2 ($Li_{0.95}Mn_2O_{3.92}$)	Rigaku Rint 2000 Cu Kα	8.2485		
					B2 ($Li_{0.98}Mn_2O_{3.94}$)		8.2436		
[11]	γ-MnO_2 + $LiOH\cdot H_2O$ 1073 K	Air	1073	Quenched	T800Q cubic + Li_2MnO_3	Neutron D2B, Grenoble	8.2449(2)	8.649(2)	1.066
			1178		T905Q tetragonal		8.1155(9)	8.6709(6)	1.068
			1198		T925Q tetragonal		8.1170(3)		
[12]	$Li_{1.07}Mn_{1.93}O_4$, Commercial (FMC Co.)	Air	933	Quenched	T-F12h330K	Synchrotron, NSLS; X18A; X7A	8.3218	8.1321	0.977 (or 1.023)[b]
					T-F3h250K		8.270	8.196	0.991 (or 1.009)[b]
[10]	$Li_2CO_3 + MnO_2$; 1073 K, 24 h × 3	Air	1178	Quenched		Scintag; Cu $K\alpha_1$	8.1155(9)	8.6486(18)	1.066
[13]	$Li_2CO_3 + 5MnO_2$; 1073 K, 8 h+	20% O_2	1073	Quenched	$\delta < 0.07$	XRD	8.2375	From graph	
		Air					8.2494		
					$0.07 < \delta < 0.15$		8.127	8.340	1.026
					$\delta > 0.15$		8.120	8.355	1.029
[14]	$Li_2CO_3 + Mn_2O_3$	O_2	1193	Quenched	Li/Mn = 0.495 ($Li_{0.99}Mn_2O_4$) + 5%Li_2MnO_3	Neutron (TOF) KENS, KEK	8.1114(4)	8.6464(5)	1.066
[15]	$Li(CH_3COO) + Mn(CH_3COO)_2$ + citric acid (sol–gel)		973	'Furnace-cooled'		Rigaku Cu Kα	8.228	8.270	1.005
			1073				8.229	8.269	1.005
[16]	α-$Mn_2O_3 + Li_2CO_3$	Air	1073	Quenched	$Li_{0.95}Mn_{2.05}O_4$	HZG3/TUR61, Fe Kα	8.32542(22)	8.14825(27)	0.979
					$Li_{0.90}Mn_{2.10}O_4$		8.1219(5)	8.6101(6)	1.060
[17]	Li_2CO_3 + Mn(III)acac, 773 K/18 h, 1173/18 h	Air, O_2	298–1253	In situ	Cubic, no phase transition	Bruker D5005, Cu Kα, HTK 1200 Anton Paar high temperature attachment	[c]		
[21]	β-MnO_2 + $LiOH\cdot H_2O$, 1123 K/20 h	Air	1123	Quenched	$LiMn_2O_4$	Philips, Cu Kα,	8.242	8.282	1.006
	1123 K/35 h	Air					8.233		
This paper	α-$Mn_2O_3 + Li_2CO_3$	Air	1073	In situ	$Li_{0.98}Mn_{2.02}O_4$; at 1073 K at 140 K	Synchrotron, Max-Lab I711	8.349042(28)		
				Quenched			8.33180(6)	8.08617(7)	0.9705

[a] All values kept or recalculated for $F4_1/ddm$ or $Fd3m$ space group.
[b] For reversed *a* and *c* parameters.
[c] The *a* lattice parameter evaluation with temperature presented graphically.

above 1393 K it is reincorporated into the spinel phase. The high temperature spinel structure samples have been defined as the $Li[Mn_2]O_4$–$Mn[Mn_2]O_4$ solid-solution members with defects in the oxygen sublattice.

Strobel et al. [11] have performed neutron diffraction investigation of $Li_{1.05}Mn_2O_{4-\delta}$ samples quenched from 1073 and 1198 K. From the Rietveld refinement, they have concluded that sample quenched from 1198 K consists of Li_2MnO_3 (9 wt%) and of the tetragonal $Li_{0.89(3)}Mn_2O_{3.84(8)}$ (91 wt%) with deficiency in the cationic tetrahedral, as well as in the anionic sublattices of the spinel structure. A sample quenched from 1073 K consists of the cubic $LiMn_2O_4$ (97.1 wt%) and Li_2MnO_3 (2.9 wt%). The obtained experimental errors suggest that for the tetragonally distorted structure the oxygen sites could be almost fully occupied, however, authors have not discussed the possibility of migration of manganese ions to tetrahedral sites.

In spite of the fact that slow cooling process usually guarantees the cubic structure of $LiMn_2O_4$ [22], the tetragonal distortion has been reported also for 'furnace-cooled' samples [15].

The tetragonal phase with c/a ratio lower than one has been reported earlier for samples quenched from a high temperature. Yang et al. [12] have indexed the X-ray patterns of the tetragonally distorted spinel phase with $c/a < 1$, but only as one of the alternative, and with a dose of uncertainty because of the multiphase system. The existence of this 'flattened' lithium–manganese spinel structure has been confirmed, using Rietveld refinement, for the members of the $Li_xMn^{(II)}_{1-x-z}Fe^{(III)}_z[Fe^{(III)}_{n(3-x)-z}Mn^{(III,IV)}_{(1-n)(3-x)+x+z-1}]O_4$ series [16].

The DSC results have revealed that the phase transition in the lithium-deficient $Li_{1-y}Mn_2O_{4-\delta}$ samples appears at higher temperature (~308 K) [20], then in the earlier reported stoichiometric $LiMn_2O_4$ (~285 K) [23].

The nature of the phase transition depends on the stoichiometry of a sample. Results presented in this paper are related to the sample with composition that gives rise to a mixture of the new 'flattened' tetragonal phase and of the orthorhombic phase. For composition with lower deficit of lithium only the orthorhombic phase was observed, whereas for higher lithium deficit one can observe the pure 'flattened' tetragonal phase, and for the highest lithium deficit the 'elongated' tetragonal phase appears [16].

2. Experimental procedure

The $Li_{0.98}Mn_{2.02}O_4$ sample was obtained by the solid-state reaction of Li_2CO_3 (99.0% Merck) with the manganese oxide precursor, α-Mn_2O_3. The precursor was prepared by precipitation of Mn-hydroxide from Mn^{2+} nitrate solution ($Mn(NO_3)_2{\cdot}6H_2O$, 99.0% Merck) with sodium hydroxide (98.8% POCH). Washed and dried at room temperature, it was dehydrated for 2 h at 523 K, and then successively at 673, 773 and 873 K for 4 h in air. Crystalline single-phase precursor displays the bixbyite (*Ia3*) structure. The spinel sample was obtained from Li_2CO_3 (Merck) and α-Mn_2O_3 powders, by reaction of the components in air at 973 K and, after grinding, at 1073 K for 4 h. Finally, the sample was quenched rapidly in the solid CO_2. The conventional laboratory X-ray powder diffraction data (Fe Kα radiation) at room temperature confirmed the formation of crystalline phase displaying cubic structure (space group *Fd3m*) and some traces of the phase with the tetragonal spinel structure (space group *$F4_1/ddm$*).

Investigations on the temperature phase transitions were carried out at the synchrotron beam-line I711 at MAX-Lab with an image foil Huber 670 Guiner camera [24] with a Cryostream Cooler (Oxford Cryosystem) and with furnace

Table 2
Structural parameters of the cubic phase resulted from Rietveld refinement of the $Li_{0.98}Mn_{2.02}O_4$ patterns collected at various temperatures

T [K]	a [Å]	V [Å^3]	Oxygen coordinates $x=y=z$	Occupancy Mn^{2+}(Tetr.)	Uiso(Tetr.) $\times 10^2$ [Å^2]	Uiso(Oct.) $\times 10^2$ [Å^2]	Uiso(oxygen) $\times 10^2$ [Å^2]	Rwp (%)	Rp (%)
260	8.24604(19)	560.707(22)	0.2574(11)	0.052				3.23	2.20
280	8.253612(28)	562.2534(33)	0.25758(13)	0.052(2)				3.70	2.80
300	8.256712(30)	562.887(4)	0.26085(6)	0.060(1)				3.39	2.31
305	8.257417(13)	563.0314(15)	0.26108(5)	0.061(1)				3.19	2.21
310	8.258043(12)	563.1595(14)	0.26123(5)	0.062(1)				3.10	2.17
320	8.259163(12)	563.3887(14)	0.26200(5)	0.045(1)	1.94(10)	0.453(7)	1.702(20)	4.00	2.81
373	8.265979(24)	564.7846(28)	0.26254(5)	0.055(1)	3.723(6)	0.589(6)	1.856(6)	3.00	2.16
473	8.277452(23)	567.1398(27)	0.26175(4)	0.056(1)	4.518(5)	0.862(5)	2.290(5)	2.75	1.98
573	8.284879(26)	568.6676(31)	0.26262(5)	0.029(1)	4.271(6)	1.137(6)	2.413(6)	3.11	2.17
673	8.298603(25)	571.4984(30)	0.26258(5)	0.037(1)	4.473(6)	1.339(6)	2.615(6)	2.89	2.06
773	8.308682(25)	573.5833(30)	0.26267(5)	0.044(1)	4.643(7)	1.509(7)	2.786(7)	2.84	2.06
873	8.318689(26)	575.6582(31)	0.26286(5)	0.049(1)	4.700(7)	1.566(7)	2.842(7)	2.92	2.09
973	8.330576(31)	578.129(4)	0.26303(6)	0.057(1)	4.759(8)	1.625(8)	2.901(8)	3.40	2.28
1073	8.349042(28)	581.9825(34)	0.26258(5)	0.090(1)	4.995(10)	1.861(10)	3.137(10)	3.13	2.27
1103	8.36540(4)	585.410(5)	0.26223(7)	0.137(1)	5.112(11)	1.978(11)	3.254(11)	3.90	2.62
1133	8.37498(5)	587.423(6)	0.26245(9)	0.163(1)	5.204(14)	2.070(14)	3.346(14)	4.69	3.05
1163	8.38928(16)	590.437(19)	0.2637(5)	0.199(10)	5.09(7)	1.96(7)	3.23(7)	9.72	5.26

The space group is *Fd3m*.

for the Huber detector in the high temperature measurements. Sample mounted in 0.3 mm capillary tubes (Hilgenberg) underwent the heating and cooling procedures in the temperature range from 110 to 1173 K. The wavelength, $\lambda = 1.08632$ Å, was determined by calibration using NIST silicon standard. The data analysis was performed with the GSAS software [25].

3. Results and discussion

3.1. Measurements at high temperature

Results for the cubic spinel phase obtained from structure refinements are summarized in Table 2. The unit-cell parameter resulting from Rietveld refinement of X-ray diffraction patterns, reveals the linear dependence of temperature in the region from room temperature to ~1073 K (Fig. 1a). At the higher temperature the lattice constant *a* increases rapidly with the temperature also in the linear fashion. Tendency to the increase of lattice constant at temperature about 1073 K is in good agreement with that reported before for its rising with calcination temperature of the $LiMn_2O_4$ sample [17,26]. Assuming linear dependence of temperature the turning point for the examined sample can be established at 1045 K.

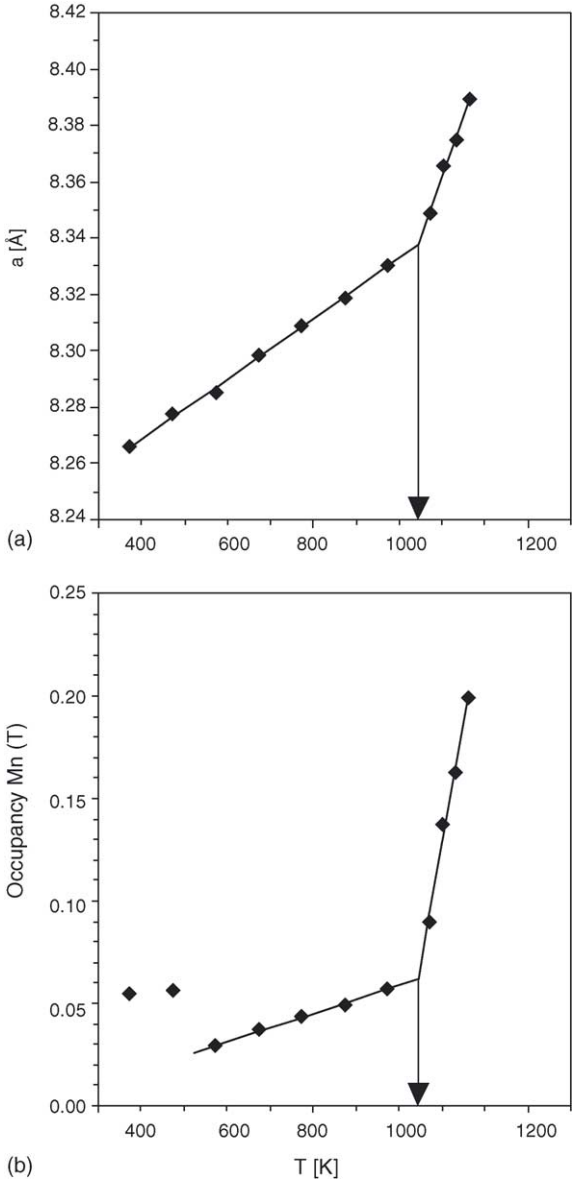

Fig. 1. The lattice parameter (a) and the fractional site occupancy (b) of Mn^{2+} ions in the *8a* tetrahedral site as a function of temperature. Straight lines were obtained from the linear fitting.

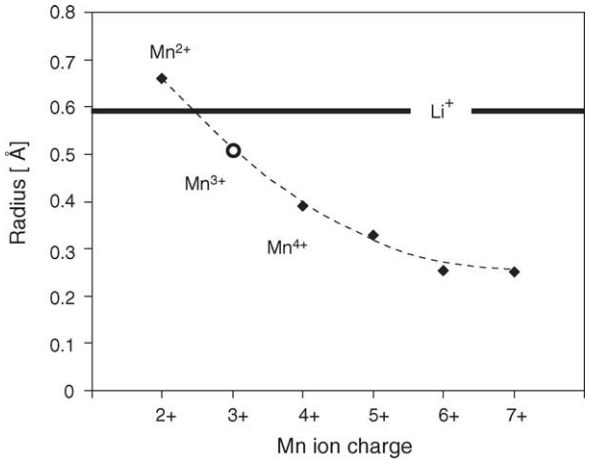

Fig. 2. The ionic radius dependence of the charge of manganese [27]. Open circles: ionic radii of Mn^{3+} from interpolation.

Because of the high crystal field stabilization of Mn^{4+} and Mn^{3+} ions on octahedral sites, the most probable cation on the tetrahedral site is Mn^{2+}. High temperature delivers the sufficient reduction condition to stabilize the Mn^{2+} ions. The comparison of ionic radii shows that only the presence of Mn^{2+} cations on tetrahedral sites can lead to the expansion of the unit-cell volume (Fig. 2).

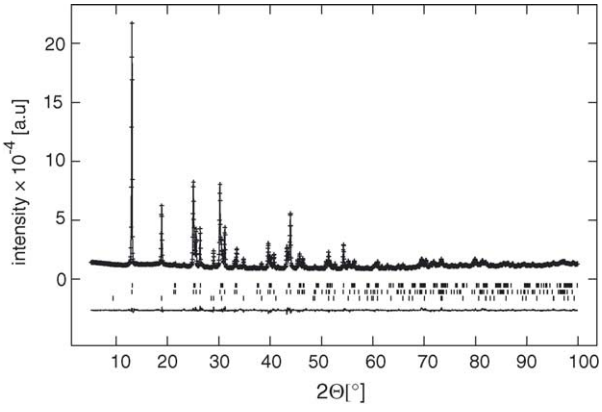

Fig. 3. Observed, calculated and difference profiles resulting from the Rietveld analysis of X-ray powder diffraction data collected on $Li_{0.98}Mn_{2.02}O_4$ sample at 140 K. The ticks show the 2Θ positions for the Bragg peaks of the orthorhombic phase (upper row), tetragonal phase (middle row) and the h-BN phase added for temperature calibration (lower row).

Fractional manganese occupancy on the tetrahedral sites, obtained from Rietveld refinement, increases rapidly above 1045 K (Fig. 1b). Both unit-cell parameter and fractional manganese occupancy of tetrahedral sites lead to the conclusion, that above 1045 K manganese ions migrate to the tetrahedral positions and reduce their oxidation state to +2. This effect corresponds well to the theoretical predictions reported earlier [28] and to the lattice constant dependence on the $LiMn_2O_4$ synthesis temperature [17,26].

In spite of the fact that the presumed chemical composition suggests fractional occupancy of 0.02 Mn on tetrahedral *8a* sites, the Rietveld refinement shows the higher manganese content on this position. The higher Mn content is comprehensible, because the sample was synthesized at 1073 K, at the temperature by about 28 K higher then the established limit. These results reveal that to control the *8a* site occupancy, the calcinations temperature should never exceed 1045 K.

The open question remains where the Li ions pushed out from the *8a* sites by Mn ions are located. There are two possibilities, both suggested by experiment and theoretical predictions [17,28]: 1) Li ions locate in the lithium-rich additional phase such as Li_2MnO_3, 2) Li ions locate on the *16c* spinel site. The planned neutron diffraction measurements should solve the problem.

3.2. New low temperature phase transition

Synchrotron X-ray diffraction pattern of the lithium deficient sample collected at 140 K shows the tetragonally distorted spinel structure, but what should be stressed, this new phase is not equivalent to the low temperature polymorph of $LiMn_2O_4$ and, in the examined sample, coexists with the well defined orthorhombic structure (space group *Fddd*) (Figs. 3 and 4). To reduce the time cost of calculations, the orthorhombic phase was indexed using 'small' unit cell (e.g. $a = 8.25846(16)$ Å, $b = 8.29055(19)$ Å, $c = 8.20103(14)$ Å for 230 K). Nevertheless, very weak superstructure reflections were observed for this minor phase, which could prove that the real structure was similar to that reported earlier for stoichiometric $LiMn_2O_4$ [29].

The results of Rietveld refinement for the pattern, collected at 140 K, are shown in Fig. 3 and the resulting structural parameters are shown in Table 3. One can see that the tetragonal structure can be satisfactorily described with the space group $F4_1/ddm$. Atomic coordinates for cation positions are: Li,

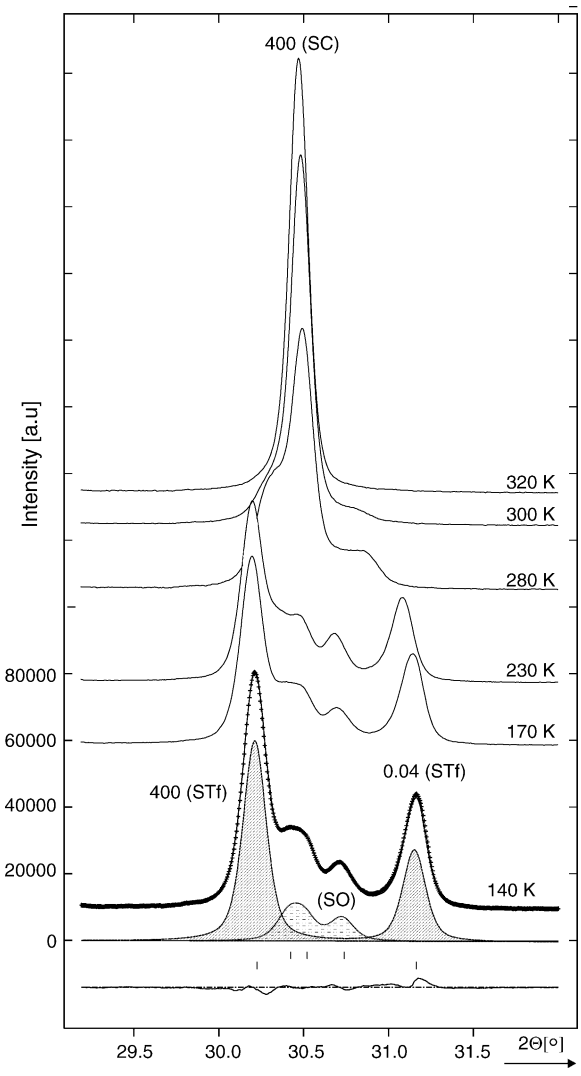

Fig. 4. The section of the graphical result of Rietveld refinement of the $Li_{0.98}Mn_{2.02}O_4$ sample at 140 K and the representative parts of the XRD patterns collected during a heating. STf: tetragonally distorted spinel structure; SO: orthorhombic spinel structure; SC: cubic spinel structure.

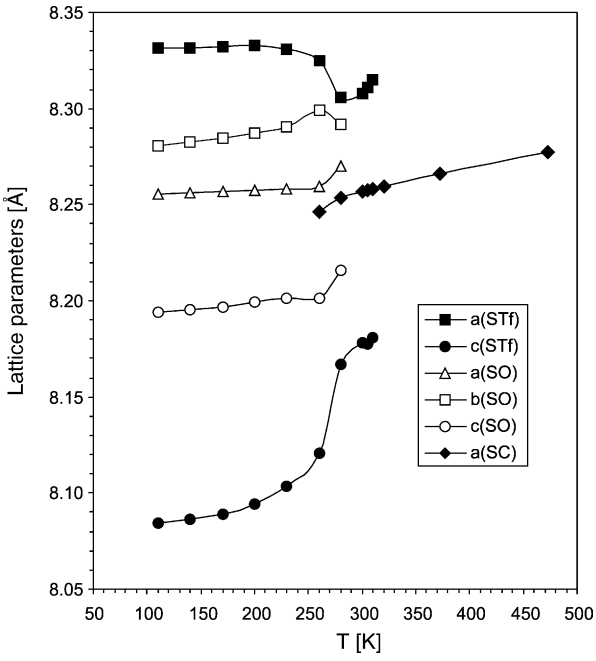

Fig. 5. Lattice parameters vs. temperature of the tetragonal (STf), orthorhombic (SO) and cubic (SC) phases as determined from Rietveld refinement analysis of SR powder diffraction data. For standard deviations compare Tables 2 and 3.

Table 3
Structural parameters of the tetragonal phase resulted from Rietveld refinement of the $Li_{0.98}Mn_{2.02}O_4$ patterns collected at various temperatures

T [K]	Unit-cell parameters		c/a	V [Å^3]	Oxygen coordinates			Interatomic distances			Occupancy Mn^{2+} (Tetr.)	Rwp (%)	Rp (%)
	a [Å]	c [Å]			x	y	z	Mn(Oct.)–O Short	Mn(Oct.)–O Long	Li, Mn(Tetr.)–O			
110	8.33145(8)	8.08407(10)	0.9703	561.140(11)	−0.01102(18)	0.01102(18)	0.26146(22)	1.9327(17)	1.9953(14)	1.9457(22)	0.347(9)	4.89	3.86
140	8.33180(6)	8.08617(7)	0.9705	561.333(8)	−0.01126(11)	0.01126(11)	0.26229(14)	1.9268(12)	1.9938(9)	1.9519(14)	0.073(3)	3.46	2.40
170	8.33235(4)	8.08918(6)	0.9708	561.617(6)	−0.01144(11)	0.01144(11)	0.26239(14)	1.9268(12)	1.9926(9)	1.9545(14)	0.074(3)	3.46	2.99
200	8.33269(6)	8.09447(8)	0.9714	562.028(8)	−0.01153(13)	0.01153(13)	0.26239(16)	1.9281(13)	1.9919(10)	1.9559(16)	0.094(3)	3.72	2.65
230	8.33104(6)	8.10324(7)	0.9727	562.415(7)	−0.01163(12)	0.01163(12)	0.26285(15)	1.9265(12)	1.9909(10)	1.9594(15)	0.083(3)	3.26	2.28
260	8.32478(4)	8.12088(6)	0.9755	562.793(6)	−0.01278(13)	0.01278(13)	0.26294(16)	1.9310(12)	1.9805(10)	1.9713(16)	0.088(3)	3.23	2.20
280	8.30560(11)	8.16709(17)	0.9833	563.391(16)	−0.0119	0.0119	0.2629				0.088	3.70	2.80
300	8.30775(17)	8.17815(27)	0.9844	564.445(25)	−0.0118	0.0120	0.2633				0.088	3.39	2.31
305	8.31121(27)	8.1778(4)	0.9839	564.89(4)	−0.0118	0.0120	0.2634				0.088	3.19	2.21
310	8.3148(5)	8.1811(8)	0.9839	565.61(7)	−0.0118	0.0121	0.2634				0.088	3.10	2.17

The space group is $F4_1/ddm$.

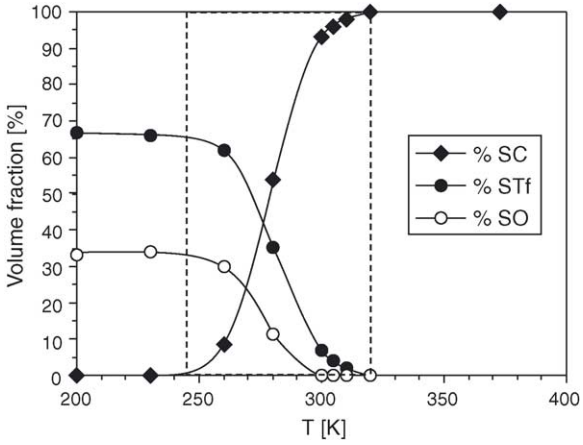

Fig. 6. The phase composition of the $Li_{0.98}Mn_{2.02}O_4$ sample as a function of temperature. Solid diamonds: % of the cubic phase (SC); solid circles: % of the tetragonal phase (STf); open circles: % of the orthorhombic phase (SO).

Mn(Tetr.) 0.875, 0.125, 0.875, Mn(Oct.) 0, 0, 0.5, the coordinates for oxygen are placed in Table 3.

Results of the accurate measurements of the spinel unit-cell parameters, for three phases in the region of phase transitions are shown in Fig. 5 and in Table 3. An anisotropic dependence of the unit-cell parameters on temperature, for the tetragonal phase differs from that observed for orthorhombic phase. The *c* parameter of the tetragonal phase increases faster than *a* and *b* parameters. On the other hand, in the orthorhombic phase the most sensitive on the temperature changes is the *b* parameter [30]. The lowering of symmetry, both in the orthorhombic phase and in the tetragonal phase, is caused by the cooperative Jahn–Teller effect, but with the different orientation and distribution of Mn^{3+} ions. The tetragonal→cubic

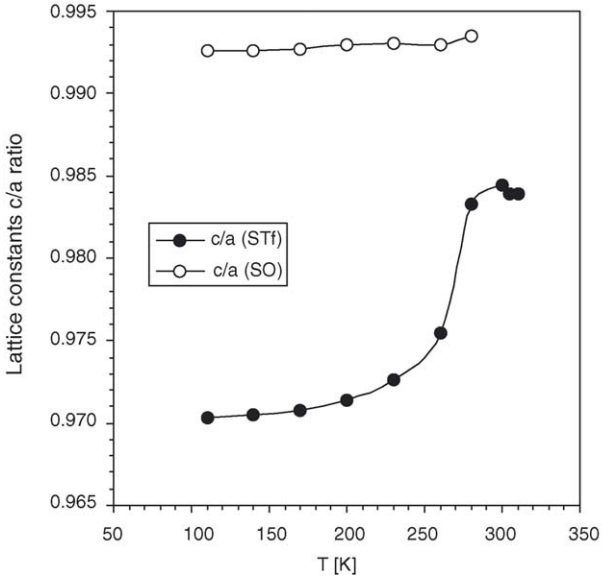

Fig. 7. The c/a ratio of the lattice parameters for the tetragonal phase ($F4_1/ddm$) (solid circles) and for the orthorhombic phase ($Fddd$) (open circles) as a function of temperature.

phase transition occurs in very wide temperature range, from ∼240 to ∼320 K (Fig. 6). Nevertheless, the variation of the *c*/*a* ratio precedes the structure transformation and can be observed in the temperature region of 110–300 K (Fig. 7).

4. Summary

Results of the synchrotron radiation X-ray diffraction measurements demonstrate that lithium deficient sample, heated up to 1173 K, maintains cubic structure, but it transforms to the tetragonal phase, when cooled down below room temperature. Therefore, the quenching procedure, which was very often used to examine the high temperature structures in ambient conditions, does not preserve the high temperature structure, but only retains the high temperature valence of manganese.

It is most interesting that the deficit of only 0.02 Li in formula $Li_{1-x}Mn_{2+x}O_4$ (or 0.7% of total cations) can involve the phase transition and it is absolutely surprising that further lithium deficit ∼0.10 Li lead to completely different phase transition. An explication of sensitivity of the $Li_{1-x}Mn_{2+x}O_4$ system to chemical composition has been given recently [16], moreover, certain additional theoretical calculations are in progress. The current paper deals with only one sample of the whole $Li_xMn_{2+x}O_4$ series. More generalization will be possible after more detailed investigations of the whole series of lithium-deficient samples.

Presented results encourage to a revision of the phase diagram of the Li–Mn–O system, and as the author believes, they accelerate the exploitation of the lithium–manganese spinel.

Acknowledgements

This work was supported by The Committee for Scientific Research KBN: grant No 4T09A 164 23 (2002–2004). I am grateful for the support from the European Community – Research Infrastructure Action under the FP6 “Structuring the European Research Area” Programme (through the Integrated Infrastructure Initiative “Integrating Activity on Synchrotron and Free Electron Laser Science”). The author would like to thank Dr. Y. Cerenius from MAX-lab (Lund) for assistance during the measurements.

References

[1] M. Nakayama, K. Watanabe, H. Ikuta, Y. Uchimoto, M. Wakihara, Solid State Ionics 164 (2003) 35.
[2] I. Yamada, T. Abe, Y. Iriyama, Z. Ogumi, Electrochem. Comm. 5 (2003) 502.
[3] M. Inaba, T. Doi, Y. Iriyama, T. Abe, Z. Ogumi, J. Power Sources 81–82 (1999) 554.
[4] I. Taniguchi, C.K. Lim, D. Song, M. Wakihara, Solid State Ionics 146 (2002) 239.
[5] D. Jugović, M. Mitrić, N. Cvjetićanin, M. Miljković, V. Jokanović, D. Uskoković, Mater. Sci. Forum 453–454 (2004) 387.
[6] Y.J. Park, J.G. Kim, M.K. Kim, H.G. Kim, H.T. Chung, Y. Park, J. Power Sources 87 (2000) 69.
[7] X.M. Wu, X.H. Li, Z. Wang, Z.B. Xiao, J. Liu, W.B. Yan, Mater. Chem. Phys. 83 (2004) 78.
[8] K.W. Kim, M.R. Kim, S.-W. Lee, K.-S. Han, S.I. Woo, Chem. Vap. Deposition 9 (2003) 187.
[9] M.M. Thackeray, M.F. Mansuetto, D.W. Dees, D.R. Vissers, Mater. Res. Bull. 31 (1996) 133.
[10] J.M. Tarascon, W.R. McKinnon, F. Coowar, T.N. Bowmer, G. Amatucci, D. Guyomard, J. Electrochem. Soc. 141 (1994) 1421.
[11] P. Strobel, F. Le Cras, L. Seguin, M. Anne, J.M. Tarascon, J. Solid State Chem. 135 (1998) 132.
[12] X.Q. Yang, X. Sun, M. Balasubramanian, J. McBreen, Y. Xia, T. Sakai, M. Yoshio, Electrochem. Solid-State Lett. 4 (2001) A117.
[13] J. Sugiyama, T. Atsumi, T. Hioki, S. Noda, N. Kamegashira, J. Alloys Compd. 235 (1996) 163.
[14] R. Kanno, A. Kondo, M. Yonemura, R. Gover, Y. Kawamoto, M. Tabuchi, T. Kamiyama, F. Izumi, C. Masquelier, G. Rousse, J. Power Sources 81–82 (1999) 542.
[15] Y.-M. Hon, K.-Z. Fung, M.-H. Hon, J. Ceram. Soc. Jpn. 108 (2000) 462.
[16] P. Piszora, W. Nowicki, J. Darul, E. Wolska, Mater. Lett. 58 (2004) 1321.
[17] V. Massarotti, D. Capsoni, M. Bini, Solid State Commun. 122 (2002) 317.
[18] R. Kanno, M. Yonemura, T. Kohigashi, Y. Kawamoto, M. Tabuchi, T. Kamiyama, J. Power Sources 97–98 (2001) 423.
[19] M. Hosoya, H. Ikuta, M. Wakihara, Solid State Ionics 111 (1998) 153.
[20] Y. Xia, T. Sakai, T. Fujieda, X.Q. Yang, X. Sun, Z.F. Ma, J. McBreen, M. Yoshio, J. Electrochem. Soc. 148 (2001) A723.
[21] P. Endres, B. Fuchs, S. Kemmler-Sack, K. Brandt, G. Faust-Becker, H.W. Praas, Solid State Ionics 89 (1996) 221.
[22] S. Ma, H. Noguchi, M. Yoshio, J. Power Sources 126 (2004) 144.
[23] G. Rousse, C. Masquelier, J. Rodríguez-Carvajal, M. Hervieu, Electrochem, Solid State Lett. 2 (1999) 6.
[24] K. Ståhl, J. Appl. Crystallogr. 33 (2000) 394.
[25] A.C. Larson, R.B. Von Dreele, Generalized Structure Analysis System (GSAS), Los Alamos National Lab. Rep. No. LAUR-86-748 (2000).
[26] J.T. Son, K.S. Park, H.G. Kim, H.T. Chung, J. Mater. Sci. 39 (2004) 3635.
[27] R.D. Shannon, Acta Crystallogr. A32 (1976) 751.
[28] Y. Koyama, I. Tanaka, H. Adachi, Y. Uchimoto, M. Wakihara, J. Electrochem. Soc. 150 (2003) A63.
[29] J. Rodríguez-Carvajal, G. Rousse, C. Masquelier, M. Hervieu, Phys. Rev. Lett. 81 (1998) 4660.
[30] P. Piszora, J. Alloys Compd. 382 (2004) 112.